Article

A Proper Shape of the Trailing Edge Modification to Solve a Housing Damage Problem in a Gas Turbine Power Plant

Thodsaphon Jansaengsuk [1], Mongkol Kaewbumrung [2], Wutthikrai Busayaporn [3] and Jatuporn Thongsri [1,*]

1   Computer Simulation in Engineering Research Group, King Mongkut's Institute of Technology Ladkrabang, College of Advanced Manufacturing Innovation, Bangkok 10520, Thailand; thodsaphon.jan@gmail.com
2   Department of Mechanical Engineering, Faculty of Engineering and Architecture, Rajamangala University of Technology Suvarnabhumi, Phranakhon Si Ayutthaya 13000, Thailand; mongkol.k@rmutsb.ac.th
3   Synchrotron Light Research Institute (Public Organization), Nakhon Ratchasima 30000, Thailand; wutthikrai@slri.or.th
*   Correspondence: jatuporn.th@kmitl.ac.th

Abstract: To solve the housing damage problem of a fractured compressor blade (CB) caused by an impact on the inner casing of a gas turbine in the seventh stage (from 15 stages), modifications of the trailing edge (TE) of the CB have been proposed, namely 6.5 mm curved cutting and a combination of 4 mm straight cutting with 6.5 mm curved cutting. The simulation results of the modifications in both aerodynamics variables C_l and C_d and the pressure ratio, including structural dynamics such as a normalized power spectrum, frequency, total deformation, equivalent stress, and the safety factor, found that 6.5 mm curved cutting could deliver the aerodynamics and structural dynamics similar to the original CB. This result also overcomes the previous work that proposed 5.0 mm straight cutting. This work also indicates that the operation of a CB gives uneven pressure and temperature, which get higher in the TE area. The slightly modified CB can present the difference in the properties of both the aerodynamics and the structural dynamics. Therefore, any modifications of the TE should be investigated for both properties simultaneously. Finally, the results from this work can be very useful information for the modification of the CB in the housing damage problem of the other rotating types of machinery in a gas turbine power plant.

Keywords: aerodynamics; compressor blade; computational fluid dynamics; computer simulation; finite element analysis; gas turbine; housing damage; power plant; structural dynamics; trailing edge

1. Introduction

In 2019, Thailand's electricity production relied on natural gas turbine power plants for up to 64% of total production. Therefore, the country's energy can be pushed into crisis whenever any of these power plants have been paused for maintenance. Consequently, avoiding the problems that may obstruct production—and maintaining every power plant to be at the highest efficiency—plays an important role in the task of maintenance engineers. Recently, one type of damage has been reported by the maintenance engineers of a power plant concerning the compressor blade (CB). The damage on the CB then causes an impact on the inner casing. This damage is also known as "housing damage" and is shown in Figure 1. Investigation showed that this damage locally occurs at the trailing edge (TE). According to the previous report, the straight cutting of TE modification at 1.0, 5.0, and 10.0 mm was proposed [1]. The computational fluid dynamics (CFD) simulation shed light on the aerodynamics (AD), pressure ratio, and change of the lift and drag coefficients (C_l and C_d) from the modifications. The results led to the conclusion that the most suitable modification was the straight cutting at 5 mm at the specific stage which caused pressure ratio alterations less than 0.2%, and the C_l and C_d changed less than 3.7% and 8.7%, respectively. This modification also maintained the aerodynamics at the same level as the original CB. This method has been applied to gas turbine power plants for actual usage

and showed steady efficiency of the power generator, as usual. However, this simple method of cutting can be improved to prolong the lifetime of the CB and also maintain the highest efficiency. In general, the original design of the CB without the modifications should be at the optimum conditions, as the production figured the structural dynamics (SD) and AD at each circumstance into the design. These parameters have been taken into account to obtain high durability and efficiency in the generator. Computer simulation has been used in an important role to study the properties of the SD, such as structural analysis, modal analysis, thermal analysis, fatigue analysis, and AD. In the details of the SD, the structural analysis can predict the profile of stress, strain, and other factors [2–7]. For modal analysis, it has been used to figure out the natural frequency, mode shape, and total deformation, among other properties [8,9]. Thermal analysis has been applied to investigate thermal stress, thermal strain, and heat transfer [7,10]. Finally, fatigue analysis has been employed to predict the damage, life, and safety factor of the CB [11,12]. For the AD, CFD can simulate the C_l, C_d, pressure, vector flow, and other variables in the compressor stage [1,13–17]. From previous computer simulations, it has been indicated that inappropriate modifications can lead to inefficiency of the generator and also shorten its lifetime. Furthermore, in [1–17], most researchers focused their study on such conditions (e.g., steady rotational speed, pressure, temperature, and flow rate). Hence, the AD study has been separated from the SD investigation, because simultaneous investigations of both the AD and the SD can be very complex and troublesome. However, various works mentioned that changes in the AD would certainly affect the SD [12,18]. In conclusion, the most suitable modification of the CB that can deliver full efficiency and sustain its level of operation requires investigations of both the AD and the SD. It is unlikely that the previous work proposed the appropriate simulation of the CB's modification, which applied these two calculations in their work.

Figure 1. Housing damage on the compressor blades in a gas turbine power plant [1]. Copyright 2019 MDPI.

In this article, we propose new shapes for CB modification in stage seven, extending further than in [1]. After that, these CBs would be investigated for whether the AD were comparable to the original and the 5 mm straight cutting ones in the identical stage using ANSYS CFX R19.2 software in a transient state. The results of the AD will be consequently input into the investigation of the SD using ANSYS harmonic response analysis, structural analysis, thermal analysis, and fatigue analysis. The results of all simulations will be analyzed to figure out the most efficient modification. The feature of this work is the proposed modification, which will be investigated in terms of both the AD and SD together under the actual operating conditions of the gas turbine power plant.

2. Theoretical Background

When the gas flows into the compressor stage, the modifications of the CB will directly change the AD and its SD properties further from the factory's design. The employed software, theory, and calculation are mentioned below.

2.1. Aerodynamics

ANSYS CFX is CFD software developed via the finite volume method (FVM), based on unsteady Navier–Stokes equations. This package is widely used to solve the problems of rotating machinery in factories [1,17,19]. The AD properties of the fluid can be found by relying on the conservation of mass for Equation (1), momentum for Equation (2), and energy for Equation (3) [20] as follows:

$$\frac{\partial \rho}{\partial t} + \nabla \cdot \left(\rho \vec{U} \right) = 0 \tag{1}$$

$$\frac{\partial \left(\rho \vec{U} \right)}{\partial t} + \nabla \cdot \left(\rho \vec{U} \otimes \vec{U} \right) = -\nabla p + \nabla \cdot \tau + \vec{S}_M \tag{2}$$

where $\vec{U}$ is the mean velocity, ρ is the fluid density, p is the pressure, $\vec{S}_M$ is the source term of momentum, and τ is the stress tensor, all of which can be related to strain rate as follows:

$$\tau = \mu \left(\nabla \vec{U} + \left(\nabla \vec{U} \right)^T - \frac{2}{3} \delta \nabla \cdot \vec{U} \right)$$

and

$$\frac{\partial (\rho h_{tot})}{\partial t} - \frac{\partial p}{\partial t} + \nabla \cdot \left(\rho \vec{U} h_{tot} \right) = \nabla \cdot (\lambda \nabla T) + \nabla \cdot \left(\vec{U} \cdot \tau \right) + \vec{U} \cdot \vec{S}_M + \vec{S}_E \tag{3}$$

where $\vec{S}_E$ is the source term of energy, λ is the thermal conductivity of the fluid, and h_{tot} is the total enthalpy, which can be related to static enthalpy $h(T,p)$ as follows:

$$h_{tot} = h(T, p) + \frac{1}{2} \vec{U}^2$$

For the turbulence equation, the shear stress transport (SST) k-ω turbulence model was chosen, as in [1,20–23]. The SST k-ω equation can be written as

$$\frac{\partial}{\partial x_j} (\rho U_j k) = \frac{\partial}{\partial x_j} \left(\left(\mu + \frac{\mu_t}{\sigma k_3} \right) \frac{\partial k}{\partial x_j} \right) + P_k - 0.09 p k \omega \tag{4}$$

$$\frac{\partial}{\partial x_j} (\rho U_j \omega) = \frac{\partial}{\partial x_j} \left(\left(\mu + \frac{\mu_t}{\sigma \omega_3} \right) \frac{\partial \omega}{\partial x_j} \right) + 1.71(1 - F_1) \frac{\rho}{\omega} \frac{\partial k}{\partial x_j} \frac{\partial \omega}{\partial x_j} + \alpha_3 \frac{\omega}{k} P_k - \beta_3 \rho \omega^2 \tag{5}$$

where μ is the molecular dynamics viscosity, P_k is the shear production of turbulence, μ_t is the eddy viscosity, ω is the specific dissipation rate, k is the turbulent kinetic energy, F_1 is the blending function, and α, β, σ are the specific coefficients for the SST k-ω turbulence model.

Further details and definitions of the parameters can be found out in [1,20–23]. The ANSYS CFX software can calculate the AD, C_l, C_d, and pressure, via Equations (1)–(5). After that, the results will be used as the input for the SD for calculation later.

2.2. Structural Dynamics

Using the results for the AD from Section 2.1, which relate to the structure of the CB, this work examines the effect on the structure by using harmonic response analysis, structural analysis, thermal analysis, and fatigue analysis based on the finite element method.

In harmonic response analysis, the AD naturally causes external frequencies which act on the CB, which can be calculated by Equation (6) [24,25] as follows:

$$\left(-\omega_f^2[M] + j\omega_f[C] + [K]\right)\{u\} = \{F\} \tag{6}$$

where ω_f is the angular frequency, $[M]$ is the structural mass matrix, $[C]$ is the structural damping matrix, $[K]$ is the structural stiffness matrix, $\{u\}$ is the nodal displacement vector, and $\{F\}$ is the load vector.

In structural analysis and fatigue analysis, the AD also causes pressure on the CB in the transient state. The structural properties, such as the total deformation, equivalent stress, and safety factor, can be calculated by Equation (7) [26]:

$$[M]\{\ddot{u}\} + [C]\{\dot{u}\} + [K]\{u\} = \{F\} \tag{7}$$

where $\{\ddot{u}\}$ is the nodal acceleration vector and $\{\dot{u}\}$ is the nodal velocity vector.

In thermal analysis, the AD also causes the temperature changes in the CB, which can be expressed as follows [27]:

$$[K(T)]\{T\} = \{Q(T)\} \tag{8}$$

where T is the temperature and $[K(T)]$ and $\{Q(T)\}$ are the thermal conduction matrix and conduction vector, respectively, which are dependent on the temperature.

3. Methodology

3.1. CB Modification

The schematic diagram of all 15 compressor stages is shown in Figure 2. This figure is not in real proportions. In the simulation, the actual CB in stage seven from the gas turbine power plant was 3D scanned (FARO Edge Arm) and modified to be a solid model as in Figure 3 (left). This solid model was then modified to be as it is in Figure 3 (right) with (a) no modification, (b) 5.00 mm straight cutting, (c) 6.50 mm curve cutting, and (d) 6.50 mm curve cutting with 4.00 mm straight cutting models. These solid models were used to investigate the AD and SD properties with the software mentioned above in Sections 2.1 and 2.2 to find out the most suitable modification in the next section.
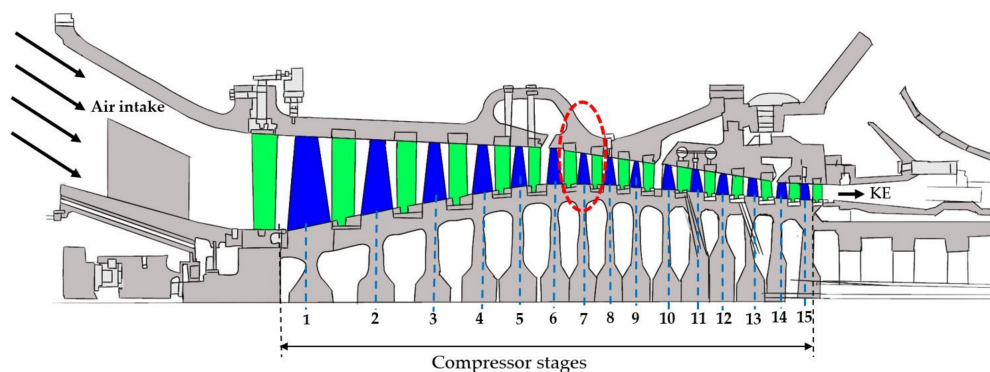

Figure 2. Schematic diagram of all 15 CBs in the compressor stages of the gas turbine power plant.
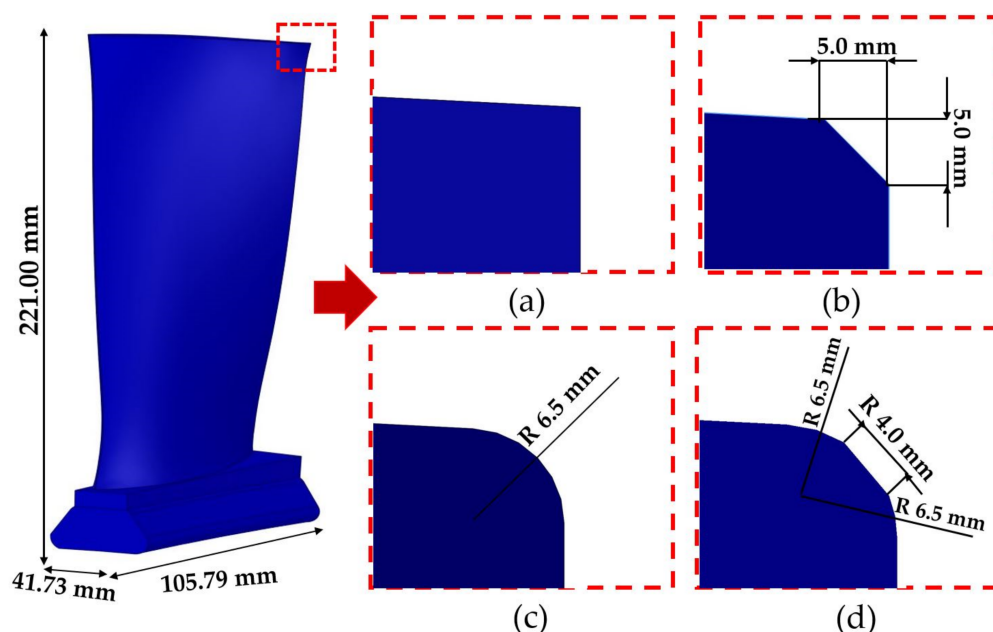
Figure 3. Solid model of the compressor blade in stage 7 from the gas turbine power plant, showing (**a**) the original design, (**b**) 5.0 mm straight cutting, (**c**) 6.5 mm curve cutting, and (**d**) 4.0 mm straight cutting with 6.5 mm curve cutting.

3.2. Models

From the models in Figure 3, the mesh model of the CB in the seventh stage was built, being composed of S6, R7, and S7. According to the complex shape of the CB, the 3D mesh model was set to be tetrahedral mesh in both the fluid's and the solid's domains. At the boundary of the two domains, an inflation was identified to be 20 layers with a y^+ of 1; the first layer thickness started at 1.41×10^{-3} mm and had a growth rate of 1.10. The inflation created wedge and prism mesh types. After that, the mesh model of the fluid domain was examined via mesh independent analysis to achieve the suitable mesh model. This model was finally adopted to build a structural mesh model later. In the independent analysis process, the maximum size of the mesh in the fluid domain was adapted to be 28–35 mm at a growth rate of 1.15. This setting caused the total elements of the mesh in both domains to be about 7.05–9.95 million elements, with the number of nodes at 2.93–3.20 million. The C_l and C_d were set to be the indicators to determine a suitable mesh model. The numbers of the elements and nodes of each model are illustrated in Table 1. In Figure 4, the mesh model of (a) the fluid's domain, (b) the interface's domain, and (c) the solid's domain of model A are shown. This model was processed with mesh independent analysis; hence, it already was suitable for further simulations. Please note that the mesh around the TE was defined with a higher number of elements than other areas because this TE was the area where the AD property would be investigated. For other models from B–D, they are similar to the model A except only on the numbers of elements and nodes. More details of the mesh independent analysis can be found in Supplementary Materials (Mesh_independent_analysis.pdf). The results of the C_l and C_d at each model exhibited differences at the third decimal places, which will be explained in Section 4.1. With the mesh independent analysis process, these indistinguishable C_l and C_d values expressed a confidential level of the mesh used in this simulation.

Table 1. Numbers of elements and nodes of each model after the mesh independent analysis (MIA) process.

Model	Fluid Domain		Solid Domain		Total	
	Element	Node	Element	Node	Element	Node
A	7,223,803	2,355,794	568,389	856,710	7,792,192	3,212,504
B	8,484,301	2,919,733	598,095	901,796	9,082,396	3,821,529
C	9,068,565	3,122,478	546,224	823,878	9,614,789	3,946,356
D	7,059,840	2,315,809	555,843	839,031	7,615,683	3,154,840
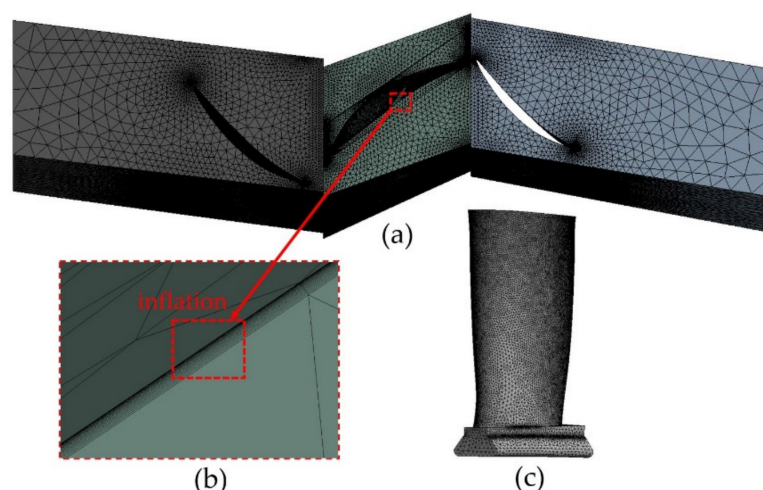
Figure 4. Mesh model of the (**a**) fluid's domain, (**b**) interface's domain, and (**c**) solid's domain of model A.

3.3. Boundary Conditions and Software Settings

The parameters to determine the boundary conditions were taken from the actual power plant and are shown in Figure 5. The gray blade is a stator, while the blue blade is a rotor. The yellow area indicates the investigating plane, which will explain the average pressure, the average temperature, and the pressure ratio for validation of the simulation in Section 4.1. The mass flow inlet was set to be 610 kg/s, and the temperature was set to be 174.15 °C. The pressure outlet was 553 kPa, while the rotation was set to 3000 rpm. Other parameters for the ANSYS CFX R19.2 software and static structural calculation are listed in Tables 2 and 3, respectively, being provided by a vendor. In the fatigue analysis, the CB was assigned to be the 422 stainless steel operating at 315 °C with the S-N curve reported in [28]. First, the calculation was in a steady state. Then, the obtained results were transferred to the transient calculation as initialized values to calculate the AD property. Finally, the AD results were applied as loads to calculate the SD property. The computational resource for simulation was 16 cores of an Intel Xeon 2.20 GHz processor with 64 GB of RAM, which required 24 h for CFD in a steady state, 120 h for CFD in a transient state, and 1.5 h for structural calculation per case. In total, it required 145.5 h per case.
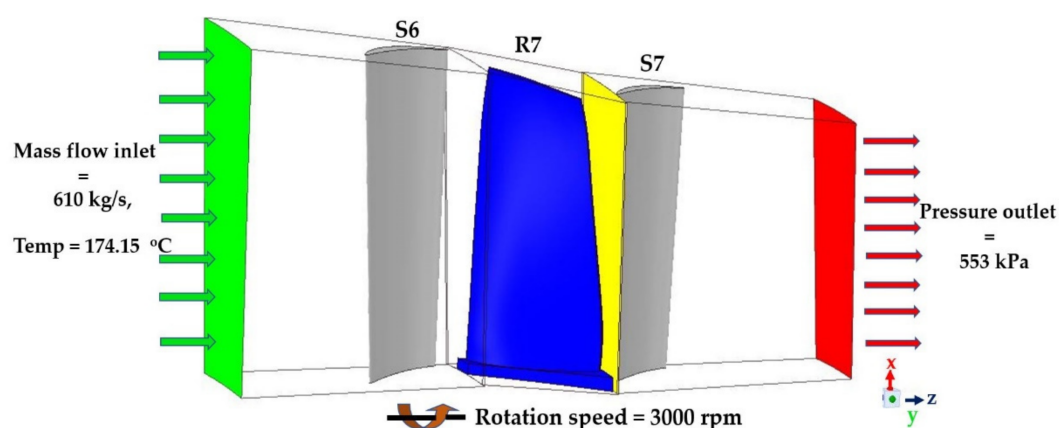
Figure 5. Boundary conditions. The positions of each blade and the observation's plan in the calculation show the (gray) stator, (blue) rotor, and (yellow) investigating plane.

Table 2. Settings and parameters for CFX calculation.

Numerical Parameters	Setting
Solvers	Pressure-based
Spatial Discretization	High-resolution scheme for the advection term
	High-resolution scheme for turbulence quantities
Convergence Control	Maximum Iteration 1000
Convergence Criteria	1.0×10^{-4}
Time Scale Control	Auto Timescale
Length Scale Option	Conservative
Time Scale Factor	Auto Timescale
Fluid	Air Ideal Gas
Heat Transfer	Total Energy
Turbulence	SST k-ω
Wall Function	High-speed (compressible) wall heat transfer model
Transient Blade Row Model	Profile Transformation
Frame Change or Mixing Model	Transient Rotor Stator
Pitch Change	Automatic

Table 3. Material's properties at 315 °C for the setting of the static structural calculation.

Property	Value
Density	7805 kg/m^3
Poisson's Ratio	0.195
Shear Modulus	79,300 MPa
Young's Modulus	1.896×105 MPa
Bulk Modulus	1.037×105 MPa
Tensile Yield Strength	1000 MPa
Tensile Ultimate Strength	1580 MPa
Thermal Conductivity	
100 °C	23.9 W/m·°C
350 °C	26.0 W/m·°C
Coefficient of Thermal Expansion	
100 °C	1.120×105 °C^{-1}
350 °C	1.147×105 °C^{-1}
S-N Curve	422 Stainless Steel [28]

4. Results and Discussion

4.1. Aerodynamics

To confirm the results of the simulation, the average pressure and the average temperature calculated at the investigating plane mentioned in Section 3.3 were compared to the

actual pressure and temperature from the vendor's measurements. The results are shown in Table 4.

Table 4. Comparison of calculated and actual pressure and temperature at the investigating plane.

Parameter	Measurement	Simulation	Error
Pressure	570,000 ± 15% Pa	619,909 Pa	8.76%
Temperature	197.0 ± 10% °C	199.3 °C	1.17%

From Table 4, the results from the simulation were consistent with the actual ones, in which the errors of the pressure and temperature were 8.76% and 1.17%, respectively. These errors are still in the confidential level of statistics. Note that the errors may have occurred because only 1.5 stages of the CB were taken into the simulation without the influence of the previous stage. In contrast, the actual measurement was probed, which took the influences of stages 1–6 into account. If the simulation included the influence of the previous stage, the errors would drastically decrease. However, by focusing on the difference in the modification of the CB, the simulation with only 1.5 stages would be sufficient. The consistency of simulation and the actual measurement confirmed the confidential level of the results.

To compare the pressures occurring in models A–D, Figure 6 has been plotted to present the pressure ratio on the investigating plane, normalized to 1 atm. The results reveal that the areas around the root and the TE of models C and D could express the pressure ratio at a similar level to model A. Contrary to this, model B had the higher pressure ratio in a larger area than the other models. Figure 6 also depicts that the modifications of the CB were strongly influential on the pressure around the root area, as reported in [1,15].
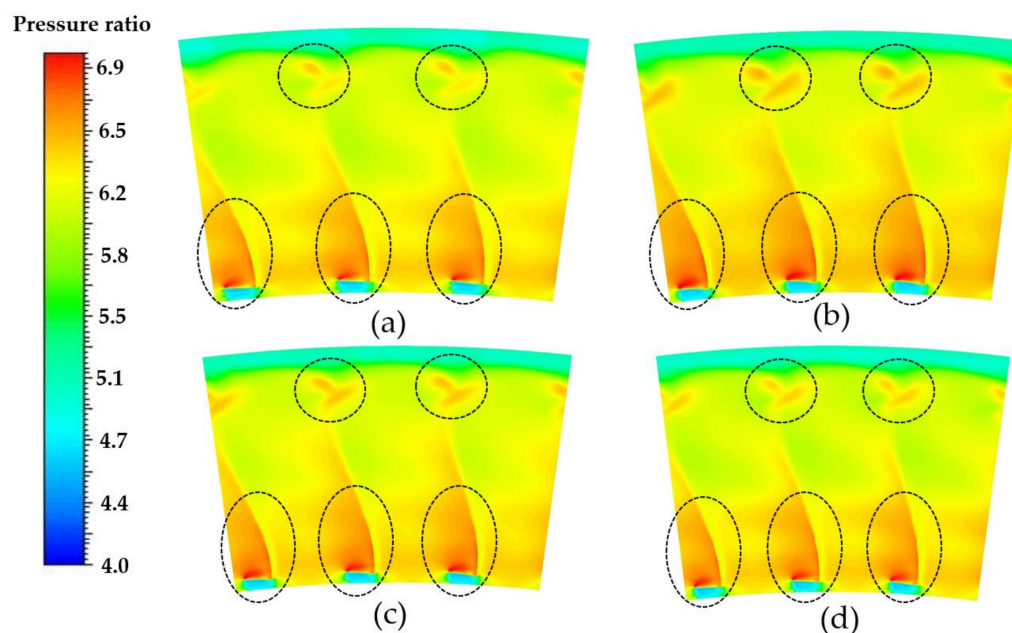

Figure 6. Pressure ratio on the investigating areas, normalized to 1 atm, for each model (**a**–**d**).

For further analysis, the results in Figure 6 were normalized with the pressure ratio of model A at the same positions and then reported in Figure 7 for blade spans of (a) 95.5%, (b) 95.8%, (c) 96.0%, and (d) 96.5%. The plots in Figure 7 have the x-axis representing the positions on the blades, while the y-axis represents the normalized pressure ratio (NPR). For the higher blade span, the position was from −0.03 m to −0.015 m, which means this position was situated close to the TE cutting. The results are also consistent with Figure 6, as the closer the positions to the TE cutting, the higher the level of the NPR found,

especially in the models B–D. Models C and D obtained comparable NPRs to model A. In contrast, model B provided the most different NPR to model A, as expected. It is noted that when the positions were closer to the TE cutting, the pressure ratio exhibited larger changes. We also found that the larger the cutting of modification, the higher the difference of the NPS, but the results did not report this here.
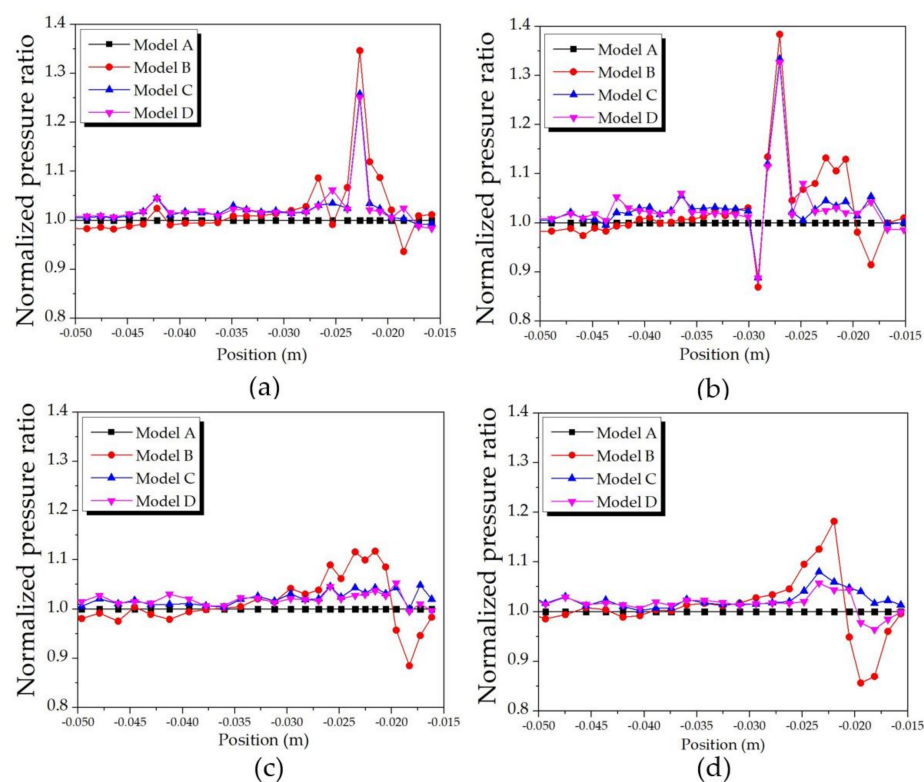

Figure 7. Plots of the normalized pressure ratio compared to blade spans of (**a**) 95.5%, (**b**) 95.8%, (**c**) 96.0%, and (**d**) 96.5%.

The AD results were used to calculate the C_l and C_d, shown in Table 5. The numbers in parentheses represent the percentage changes compared with the results of model A. The C_l and C_d could be altered up to 3.67% and 2.18%, respectively. It might be concluded that the modifications proposed in this work had an insignificant effect on the changes of the C_l and C_d. Model C led to C_l and C_d values more similar to those in model A than the other models, corresponding to the pressure ratio and the NPR reported in Figures 6 and 7.

Table 5. Result of the C_l and C_d for each model and the necessary parameters for calculation.

Model or Parameter	F_z (N)	F_y (N)	Area (m²)	C_l	C_d
A	762.945	712.282	0.0415014	0.245	0.229
B	740.563	702.746	0.0414735	0.234 (−3.67%)	0.227 (−0.87%)
C	744.547	701.989	0.0414946	0.240 (−2.04%)	0.226 (−1.31%)
D	766.729	717.477	0.0414903	0.250 (+2.04%)	0.234 (+2.18%)

To determine the effect of the AD on the structure, Figure 8 shows the distributions of the (a) pressure load and (b) temperature load for model A, calculated from the AD and the boundary conditions mentioned in Section 3.3. In the actual operation of the CB, the pressure and the temperature increased in every higher stage. However, the results show that the pressure and the temperature of the CB in each position were not identical and became higher at the TE. In Figure 8a, the average pressure on the blade was about 687,574 Pa, while the pressure around the TE could be up to 1 MPa. Similarly, Figure 8b

exhibits that the average temperature on the CB was approximately 234 °C, but the TE area presented a temperature much higher at 280 °C. Models B–D could provide a similar trend to the results. The pressure and temperature loads from the AD are important data and should be of concern.
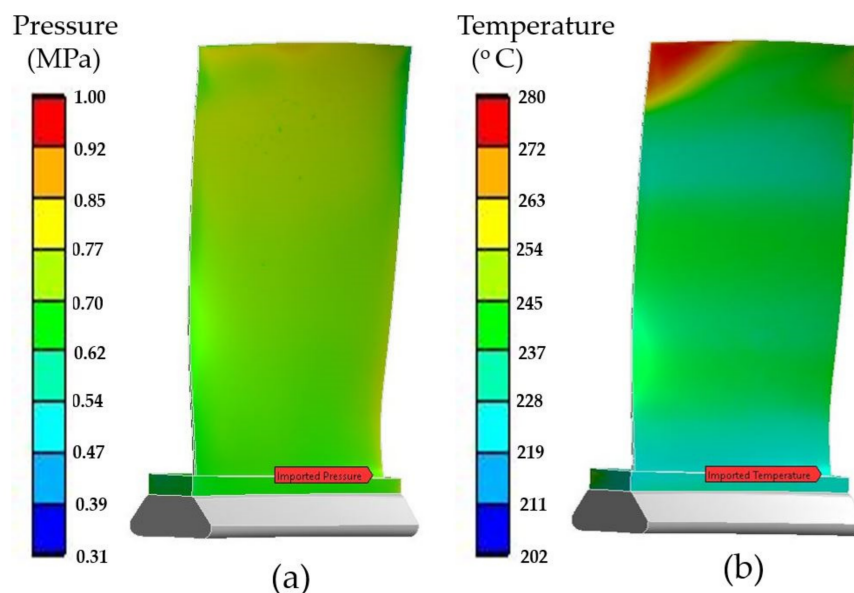

Figure 8. Distribution of the (**a**) pressure load and (**b**) temperature load of model A, calculated from the AD and the boundary conditions.

4.2. Structural Dynamics

To investigate the structural properties using harmonic response analysis, the pressure loads of models A–D in Figure 8a were averaged and then plotted in terms of the time domain, as shown in Figure 9a, from 0.00 to 0.02 s. Please note that the times later than 0.02 also exhibited similar results. After that, the results in Figure 9a would be calculated using a fast Fourier transform (FFT) and then normalized with the maximum pressure to obtain the normalized power spectrum (NPS) as in Figure 9b. This NPS could be the indicator to precisely investigate the frequency, as mentioned in [29]. From the results in Figure 9a, it was confirmed that the shapes of the modifications affected the average pressure. In Figure 9b, the pressure caused by the AD could be distinguished in terms of frequencies as 50, 100, 150, 200, 250, 300, and 350 Hz, corresponding to the value of the NPS. There was no frequency higher than 350 Hz that would react on the CB. These frequencies were caused by the rotational movement of the gas turbine at 3000 rpm, which was dominated by a 50 Hz fundamental frequency and composed of other frequencies as the harmonic frequencies. The CB's modification rarely affected the frequency. To analyze the total deformation, the 50 Hz frequency was taken into account using harmonic response analysis. The results can be seen in Figure 10. It was demonstrated that the maximum of the total deformation could be up to 1.12 mm. Moreover, most of the positions in every model showed an insignificant amount of deformation, which means the modifications had no influence on the harmonic frequency. For the higher frequencies, the effect of deformation also decreased.
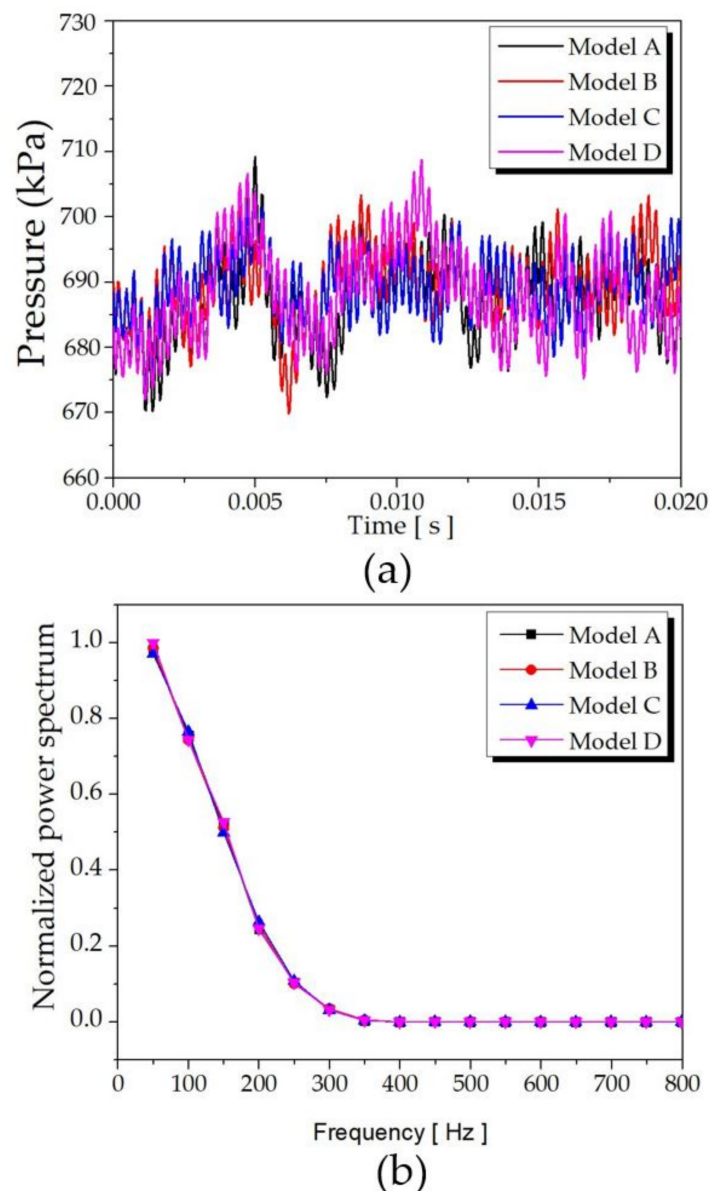
Figure 9. Plots of the (**a**) pressure load in the time domain and (**b**) NPS after the FFT and normalized by the maximum pressure.

To investigate the effect of the AD on the structure, Figure 11 shows the (a) total deformation (TD) and (b) equivalent von Mises stress (ES) from the pressure load and temperature of the AD, calculated using thermal analysis. In Figure 11a, the TD occurred at a higher rate near the upper part of the CB, while the ES occurred near the root of the CB. These results are also consistent with [30], which reported only the results in the structural simulation without loads from the AD. Furthermore, our work took the actual industrial parameters into account and provided more details than [30]. In addition, the simulation showed that with the loads that were applied, the TD and ES would be increased compared with the cases without the loads. The ES with loads appeared to be higher in the root area than the CB without loads, as expected. Our suggestion also mentions the computer simulation, as it should apply both the AD and the SD into the simulation for precise prediction, as in this work. Figure 12 reveals the TD in various models, considering only the area around the TE. We found that the TD had a similar pattern for all models. The modification did not affect the TD of the CB. From Figures 11 and 12, the maximum thermal expansion was discovered to be 3.70 mm at the leading edge, compared with the expansion

at the TE of 2.62 mm. From Figure 2, the clearance between the inner casing and the TE was 5.20 mm, while the clearance between the inner casing and the leading edge was 6.80 mm. These expansions caused gaps between these parts, reduced to be 3.10 mm and 2.58 mm at the leading edge and the TE, respectively. If other factors had been included in the calculation, such as the vibration and expansion caused by the harmonic frequencies mentioned in Figure 10, the clearance, especially at the TE, would not be sufficient and lead to housing damage. Therefore, the larger gaps from the modification could dispute this problem at the leading edge. Figure 13 displays the ES in various models. It can be found that in every model, the ES had insignificant differences; hence, the modification of the TE had no effect on the ES at the edge area, only playing an important role at the root. As seen in Figure 2, the dimension of each CB was different. Hence, the length of the TE's cutting may be varied. From the results of the calculations, it can be confirmed that curved cutting was the proper choice for CB modification.
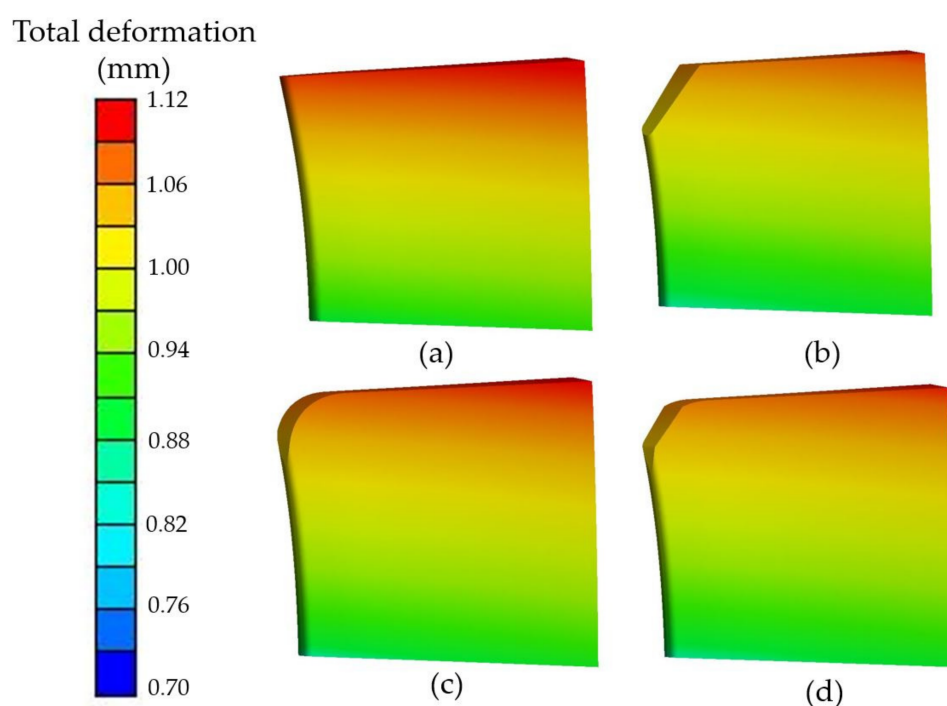

Figure 10. Total deformation on the trailing edge of (**a**) model A, (**b**) model B, (**c**) model C, and (**d**) model D at a 50 Hz frequency using harmonic response analysis calculation.

Figure 14 demonstrates the safety factors of the CB, calculated by fatigue analysis, for models A–D. The picture to the left (right) shows the plot of the safety factor for the unmodified CB (various modified CBs). As in the CB operation, a high fatigue cycle occurred. However, this work found that the modifications had no influence on the safety factor. On the other hand, every model showed the lowest safety factor around the root area. The reason for this is that the root area was the area where the CB had been plugged into the socket of the generator (see Figures 1 and 2). Therefore, the combinations of stress from rotation, compression from the CB attached to other components, thermal expansion, and temperature loads reacted to this area. These could cause the highest chance of damage happening. The safety factor around the root thus exhibited the low values of 0–1 at the surface. For further analysis into the axis, the safety factor drastically increased up to 15, which indicated that the deeper area had no chance of damage. This could be consistent with the actual results in Figure 1 (right picture) and the simulation results in Figure 16 in [12]. In more detail, the right section of Figure 1 clearly demonstrated the traces, scratches, and erosions around the root area. All of these agreements confirmed

the consistency of the calculated safety factor and indicated that the modifications could be applied to the CB and had no effect on its operational lifetime.
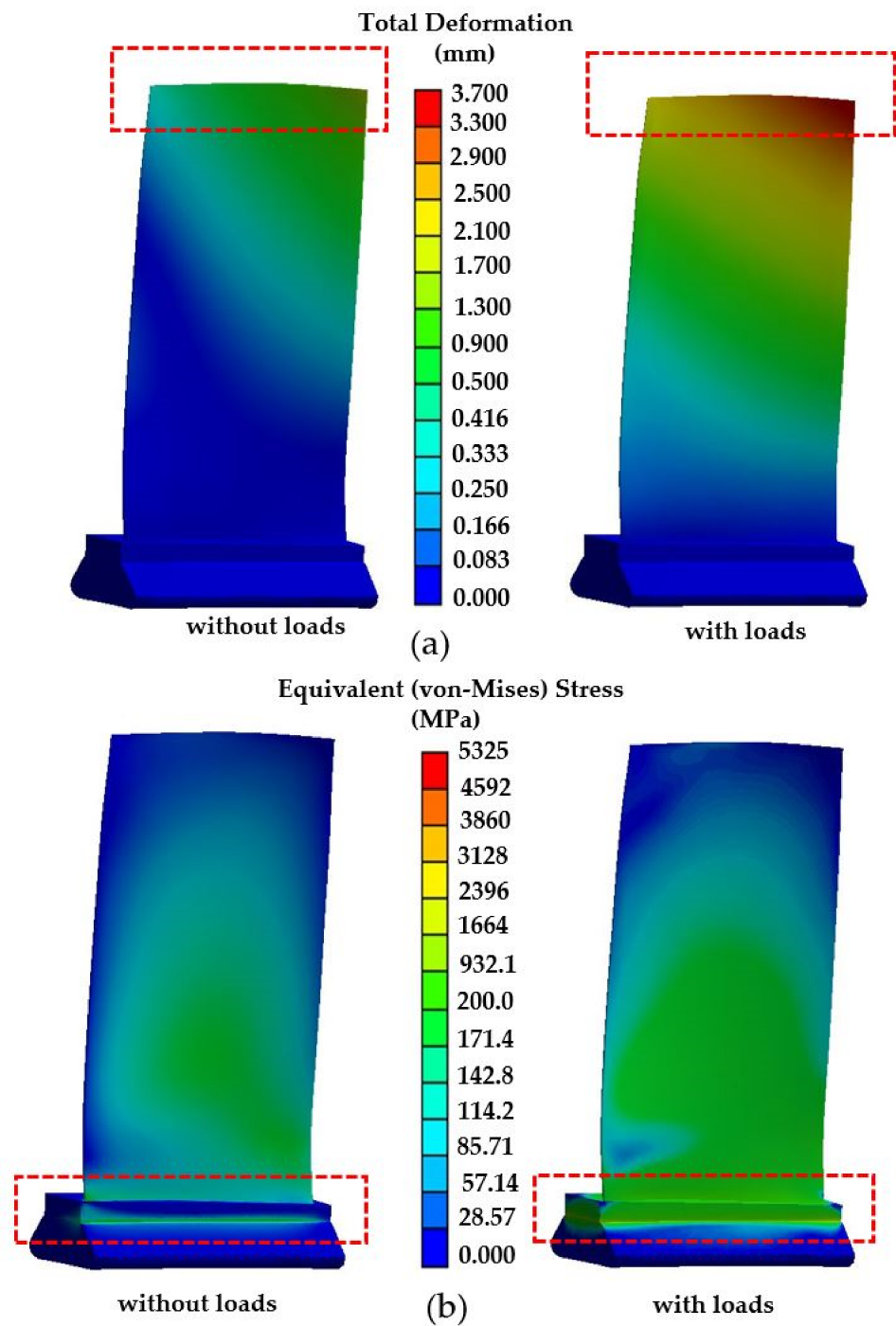

Figure 11. (**a**) Total deformation (TD) and (**b**) equivalent (von Mises) stress with and without pressure and temperature loads.
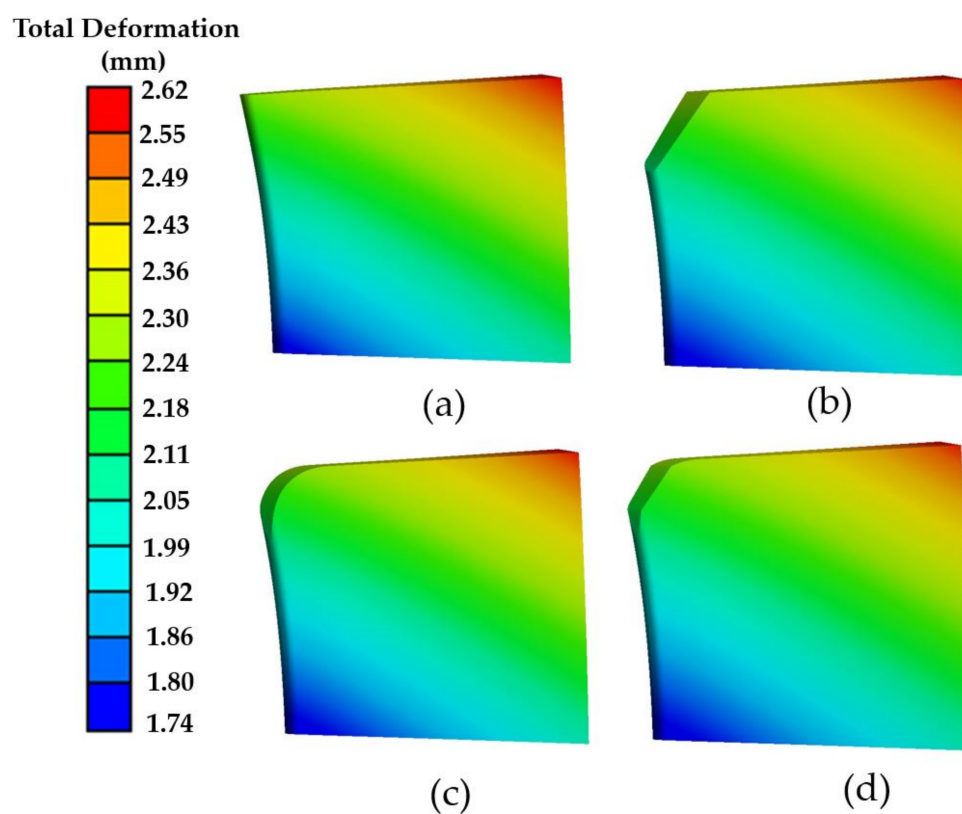
Figure 12. Total deformation on the trailing edge of (**a**) model A, (**b**) model B, (**c**) model C, and (**d**) model D, considering only the trailing edge area.
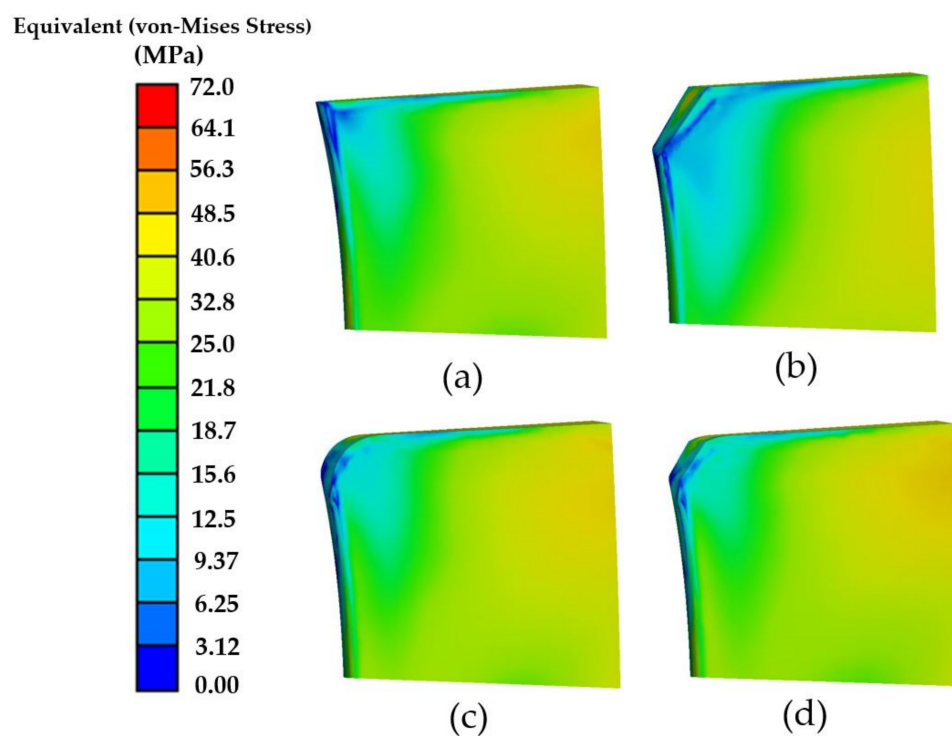

Figure 13. Equivalent von Mises stress in (**a**) model A, (**b**) model B, (**c**) model C, and (**d**) model D.
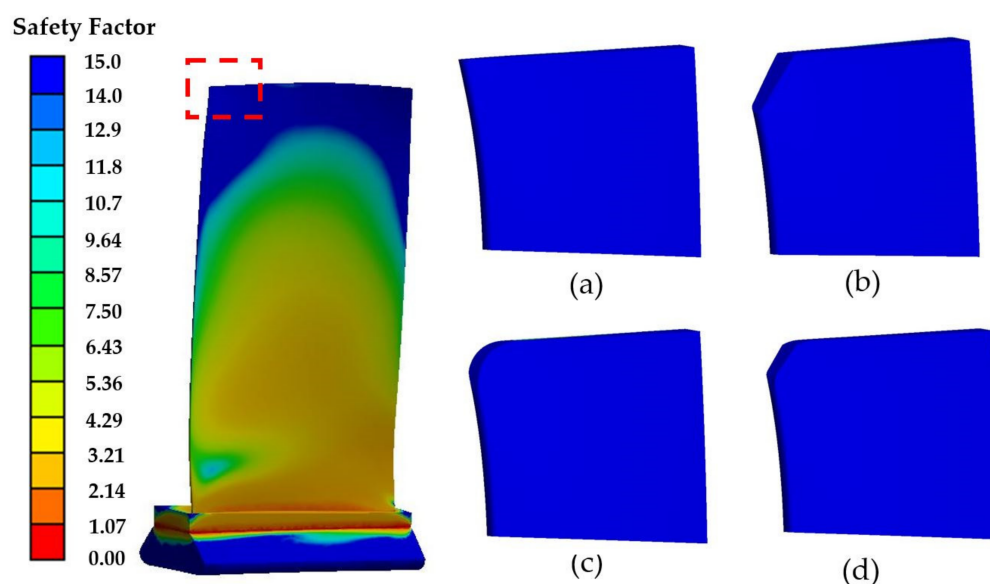
Figure 14. Safety factor on the trailing edge of (**a**) model A, (**b**) model B, (**c**) model C, and (**d**) model D.

From all the calculations of the AD and SD, the results led to the conclusion that models B, C, and D could be the solution to the housing damage. Model C obtained similar results to model A, considering the AD parameters such as the C_l, C_d, and pressure ratio. Moreover, considering the SD properties, such as the TD, ES, NPS, and safety factor, all models exhibited similar results. On the other hand, model B provided more unpleasant results in the AD than models C and D. In conclusion, model C was shown to be the most suitable model, considering the factor of uncomplicated modification and maintenance. Recently, this result has been applied for real use in a gas turbine power plant.

5. Conclusions

To solve the housing damage problem that happened in stage seven of the compressor stage in the gas turbine, this research proposed decent modifications of a CB composed of 6.5 mm curve cutting and the combination of 4 mm straight cutting with 6.5 mm curve cutting. These two models were simulated for their AD and structural properties. Using ANSYS CFX R19.2 with the SST k-ω turbulence model in the transient state, the AD results showed that the 6.5 mm curve cutting CB delivered results for the pressure ratio, C_l, C_d, and normalized power spectrum similar to the original CB. This modification also presented better results than the previous 5 mm straight cutting model and the combination of the 4 mm straight cutting with 6.5 mm curve cutting model. The consistency of all pressure and temperature values from the simulations and the measurements confirmed the confidence of the work. After that, the results of the AD were taken into account for the structural calculations, such as the structural analysis, harmonic response analysis, thermal analysis, and fatigue analysis using ANSYS structural analysis. The simulations revealed the increase of the pressure and temperature from the boundary conditions, especially at the upper edge of the CB. Therefore, in any modifications to the design and development of rotating machinery, the trailing edge area and upper edge should be investigated for both their AD and SD properties simultaneously. Then, the pressure from the aerodynamics calculations were used with a FFT and harmonic response analysis. The calculations found that the modifications had an insignificant influence on the harmonic frequency, total deformation, and equivalent stress. Then, the results from the AD were transferred to the thermal analysis and fatigue analysis. The results showed that the modification did not affect the SD properties, such as the total deformation, equivalent stress, and safety factor. A proper model with 6.5 mm curve cutting was proposed to be the most suitable model to be applied to actual modifications in the factory. This model has been proven to be the solution for the housing damage problem.

Abbreviations

i, j	1, 2, and 3 correspond to x, y, and z, respectively
AD	aerodynamics
ω_f	angular frequency (rad/s)
F_1	blending function
μ_t	eddy viscosity (m^2/s)
ρ	density (kg/m^3)
$\{F\}$	load vector (N)
$\overrightarrow{U}$	mean velocity (m/s)
μ	molecular dynamics viscosity (Pa s)
$\{\ddot{u}\}$	nodal displacement vector (m)
$\{u\}$	nodal displacement vector (m)
$\{\dot{u}\}$	nodal velocity vector (m/s)
p	pressure (Pa)
P_k	shear production of turbulence
$\overrightarrow{S}_E$	source term of energy (N/m^2 s)
$\overrightarrow{S}_M$	source term of momentum (N/m^3)
α, β, σ	specific coefficient for SST k-ω
ω	specific dissipation rate (1/s)
τ	stress tensor (Pa)
$[C]$	structural damping matrix (N s/m)
SD	structural dynamics
$[M]$	structural mass matrix (kg)
$[K]$	structural stiffness matrix (N/m)
T	temperature (°C)
$[K(T)]$	thermal conduction matrix (W/°C)
λ	thermal conductivity (W/m K)
$\{Q(T)\}$	thermal conduction vector (W)
h_{tot}	total enthalpy (J)
k	turbulent kinetic energy (J/kg)

References

1. Kaewbumrung, M.; Tangsopa, W.; Thongsri, J. Investigation of the Trailing Edge Modification Effect on Compressor Blade
   Aerodynamics Using SST k-ω Turbulence Model. *Aerospace* **2019**, *6*, 48. [CrossRef]
2. Amoo, L.M. On the design and structural analysis of jet engine fan blade structures. *Prog. Aerosp. Sci.* **2013**, *60*, 1–11. [CrossRef]

3.   Heidari, M.; Amini, K. Structural modification of a steam turbine blade. *IOP Conf. Ser. Mater. Sci. Eng.* **2017**, *203*, 012007. [CrossRef]

4.   Pugachuk, A.S.; Muller, D.V.; Fominyh, N.K. Development of impellers based on prototypes in microturbine plants. *AIP Conf. Proc.* **2019**, *2141*, 030031.

5.   Zhu, M. Design and analysis of steam turbine blades. *J. Phys. Conf. Ser.* **2019**, *1300*, 012056. [CrossRef]

6.   NithinKumarK, C.; Tandon, T.; Silori, P.; Shaikh, A. Structural Design and Analysis of Gas Turbine Blade using CAE tools. *Int. J. Eng. Res. Technol.* **2014**, *3*, 469–474.

7.   Ujade, G.; Bhambere, M. Review of Structural and Thermal Analysis of Gas Turbine Blade. *Int. J. Mech. Eng. Robot. Res.* **2014**, *3*, 347.

8.   Singh, H.P.; Rawat, A.; Manral, A.R.; Kumar, P. Computational analysis of a gas turbine blade with different materials. *Mater. Today Proc.* **2020**. [CrossRef]

9.   Boudounit, H.; Tarfaoui, M.; Saifaoui, D. Modal analysis for optimal design of offshore wind turbine blades. *Mater. Today Proc.* **2020**, *30*, 998–1004. [CrossRef]

10.   Boyaraju, G.; Rajasekhar, S.; Sridhar, A.; Rao, J. Thermal analysis of a gas turbine rotor blade. *Int. J. Sci. Eng. Adv. Technol.* **2015**, *3*, 1181–1187.

11.   Ngoret, J.K.; Kommula, V.P. Comprehending Occurrence of Premature Failure in Compressor Turbine (CT) Blades for Short-Haul Aircraft Fleet. *Int. J. Eng. Res. Afr.* **2019**, *42*, 10–23. [CrossRef]

12.   Kou, H.J.; Lin, J.S.; Fu, X. Dynamic and fatigue compressor blade characteristics during fluid structure interaction: Part I-Blade modelling and vibration analysis. *Eng. Fail. Anal.* **2017**, *76*, 80–98. [CrossRef]

13.   Zhu, F.-w.; Ding, L.; Huang, B.; Bao, M.; Liu, J.-T. Blade design and optimization of a horizontal axis tidal turbine. *Ocean Eng.* **2020**, *195*, 106652. [CrossRef]

14.   Cui, B.; Zhang, C.; Zhang, Y.; Zhu, Z. Influence of Cutting Angle of Blade Trailing Edge on Unsteady Flow in a Centrifugal Pump Under Off-Design Conditions. *Appl. Sci.* **2020**, *10*, 580. [CrossRef]

15.   Lu, J.L.; Chu, W.; Zhang, H. Influence of blade tip cutting on axial compressor aerodynamic performance. *Proc. Inst. Mech. Eng. Part G J. Aerosp. Eng.* **2009**, *223*, 19–29. [CrossRef]

16.   Möller, D.; Jüngst, M.; Holzinger, F.; Brandstetter, C.; Schiffer, H.-P.; Leichtfuß, S. In Numerical Investigation of Tip Clearance Flow Induced Flutter in an Axial Research Compressor. In *ASME Turbo Expo 2016: Turbomachinery Technical Conference and Exposition*; American Society of Mechanical Engineers Digital Collection: New York, NY, USA, 2016.

17.   Halder, P.; Kumar, P.M. Coupled CAD-CFD automated optimization for leading and trailing edge of an axial impulse turbine blade. *Ocean Eng.* **2020**, *213*, 107769. [CrossRef]

18.   ANSYS, Inc. Lecture 01: Overview of FSI in Workbench. In *ANSYS Fluent Fluid-Structure Interaction (FSI) with ANSYS Mechanical*; ANSYS Inc.: Canonsburg, PA, USA, 2016.

19.   ANSYS, Inc. ANSYS 17.1. In *ANSYS CFX Introduction*; ANSYS Europe Ltd.: Canonsburg, PA, USA, 2017.

20.   ANSYS, Inc. *CFX-Solver Theory Guide R19.2*; ANSYS Inc.: Canonsburg, PA, USA, 2019.

21.   Menter, F.R. Two-equation eddy-viscosity turbulence models for engineering applications. *AIAA J.* **1994**, *32*, 1598–1605.22. [CrossRef]

22.   Puangburee, L.; Busayaporn, W.; Kaewbumrung, M.; Thongsri, J. Evaluation and Improvement of Ventilation System Inside Low-Cost Automation Line to Reduce Particle Contamination. *ECTI Trans. Electr. Eng. Electron. Commun.* **2020**, *18*, 35–44. [CrossRef]

23.   Santati, S.; Thongsri, J.; Sarntima, P. Modified small-volume jet nebulizer based on CFD simulation and its clinical outcomes in small asthmatic children. *J. Healthc. Eng.* **2019**, *2019*, 2524583. [CrossRef]

24.   Tangsopa, W.; Thongsri, J. Development of an industrial ultrasonic cleaning tank based on harmonic response analysis. *Ultrasonics* **2019**, *91*, 68–76. [CrossRef] [PubMed]

25.   Tangsopa, W.; Thongsri, J. A Novel Ultrasonic Cleaning Tank Developed by Harmonic Response Analysis and Computational Fluid Dynamics. *Metals* **2020**, *10*, 335. [CrossRef]

26.   ANSYS, Inc. ANSYS 2020 R1. In *ANSYS Mechanical APDL Theory Reference*; ANSYS Europe Ltd.: Canonsburg, PA, USA, 2020.

27.   ANSYS, Inc. Module 07: Modal, Thermal, and Multistep Analysis. In *Introduction to ANSYS Mechanical*; ANSYS Inc.: Canonsburg, PA, USA, 2016.

28.   Briggs, J.Z.; Parker, T.D. The super 12% Cr Steels. In *Source Book on Materials for Evaluated-Temperature Applications*; Elihu, F.B., Ed.; American Society for Metals: Geauga County, OH, USA, 1979; p. 121.

29.   Tangsopa, W.; Thongsri, J. A Dual Frequency Ultrasonic Cleaning Tank Developed by Transient Dynamic Analysis. *Appl. Sci.* **2021**, *11*, 699. [CrossRef]

30.   Kumar, R.R.; Pandey, K.M. Static Structural and Modal Analysis of Gas Turbine Blade. *IOP Conf. Ser. Mater. Sci. Eng.* **2017**, *225*, 012102. [CrossRef]